

Short communication

Acid treated Sr-substituted LaCoO₃ perovskite for toluene oxidationYonghui Wei^{*}, Lei Ni, Minxia Li, Jili Zhao

College of Chemistry and Biology, Beihua University, Jilin 132013, PR China



ARTICLE INFO

Keywords:

Toluene oxidation
Perovskite
Sr segregation
Acid treatment

ABSTRACT

For A-site substituted AA'BO₃ perovskite, the doped A' element is easy to migrate to the surface and form segregation of A'O_x, which could partially block active B sites and thus reduce catalytic activity. In the present work a La_{0.8}Sr_{0.2}CoO_{3-δ} perovskite-type solid was first prepared and then treated with acetic acid to eliminate SrO segregation on its surface. The obtained catalyst (LCSO-a) possessed a significantly enhanced catalytic activity for toluene oxidation in the 220–260 °C range. This promotion effect might be attributed to the increase in the concentration of active surface oxygen species and the reduction in their binding strength. In addition, the LCSO-a catalyst showed very good stability and water resistance.

1. Introduction

As a derivative of benzene and one of typical volatile organic compounds (VOCs), toluene is a commonly used solvent in the chemical industry and a significant contributor to the formation of photochemical smog [1–3]. Among the current technologies for VOCs elimination, such as toluene, catalytic oxidation has been considered as one of the most effective due to its low operation temperature, high purification efficiency, recoverable heat, and no secondary pollution [4–8]. Traditional catalysts of noble metals usually exhibit higher catalytic activity compared with those of metal oxides. However, their high cost and significant poisoning tendency limit their further considerations for VOCs catalytic applications [9–11]. Therefore, the development of new and efficient catalysts is a research hotspot in VOCs emission control technology.

Perovskites, with the general formula ABO₃, are considered promising candidates for replacing noble metals in several heterogeneous catalytic applications due to their flexible composition, good redox properties, superior thermal stability, and relatively low price [12–15]. However, the catalytic performance of ABO₃ is usually not satisfactory in the case of VOCs oxidation reactions. Many methods were used to improve their activities in recent years [16–20]. The most common approach is to substitute A site with a lower valence A' cation to tune the valence of B site or enhance the mobility of active surface oxygen species. Weng et al. [21] synthesized Ca²⁺ and Mg²⁺ modified LaCoO₃ perovskites and found that the introduction of Ca²⁺ and Mg²⁺ were beneficial for the toluene oxidation process, which reduced significantly the apparent activation energy (*E_a*) of LaCoO₃ to only 34 kJ/mol. Chang

et al. [22] prepared LaMnO₃ perovskites and Sr²⁺- and Cu²⁺-doped perovskites with enhanced catalytic activity for phenol oxidation. On the other hand, it has been recently proposed that doped A' cation may partially migrate from the bulk to the surface of perovskite (surface segregation) [23,24]. Shao-Horn and co-workers [23] found that Sr segregation emerged and the SrO/La_{0.8}Sr_{0.2}CoO_{3-δ} structure was formed when Sr was doped into the LaCoO₃. B site (transition metal element) is considered as the active site of ABO₃ in VOCs oxidation [25–27], and Sr segregation on the surface of La_{0.8}Sr_{0.2}CoO_{3-δ} would partially cover active B sites, and therefore reducing catalytic activity.

The A-site doping in perovskites brings two aspects of influencing the VOCs oxidation. In one hand, the valence of B site is tuned, or the mobility of active surface oxygen is enhanced, which both benefit the improvement of catalytic activity. On the other hand, the doped A' site is easy to migrate to the surface and form A'O_x segregation, which could partially block active B sites and thus deteriorate the catalytic activity. The synthesis temperature is one of the key factors that influence the formation of A'O_x segregation [24]. Usually, the negative effect is weaker than the positive effect, and the catalytic performance is enhanced after A-site doping. It appears to the best of our knowledge that not so much attention was given to the negative effect in the literature.

Here, LaCoO₃ (LCO) perovskite was doped with Sr and La_{0.8}Sr_{0.2}CoO_{3-δ} (LSCO) was formed at a high-temperature (900 °C) treatment to enlarge the negative effect. The La_{0.8}Sr_{0.2}CoO_{3-δ} showed lower catalytic activity than LaCoO₃ in toluene oxidation. Subsequently, a selective method for the removal of surface SrO was adopted (Scheme 1). The obtained catalyst (LCSO-a) showed a remarkably improved catalytic

^{*} Corresponding author.

E-mail address: bhxwyh@163.com (Y. Wei).

<https://doi.org/10.1016/j.catcom.2021.106314>

Received 16 November 2020; Received in revised form 31 March 2021; Accepted 4 April 2021

Available online 7 April 2021

1566-7367/© 2021 The Author(s).

Published by Elsevier B.V. This is an open access article under the CC BY-NC-ND license

(<http://creativecommons.org/licenses/by-nc-nd/4.0/>).

activity. H₂-TPR and XPS were carried out to gather information about possible reasons for the different catalytic performance of the three perovskite-type materials investigated for toluene oxidation. It is the first time the influence of A'O_x segregation and the effective solution to such a negative effect in VOCs oxidation is investigated to the best of our knowledge. The results of this work provide an effective way for the A-site doped perovskites materials to show their intrinsic catalytic activities in VOCs oxidation.

2. Experimental

2.1. Synthesis of monodisperse PMMA microspheres

Monodisperse polymethyl methacrylate (PMMA) microspheres were used as the hard template. At first, 3.0 mmol K₂S₂O₈ was added into a three-necked flask with 1500 mL deionized water at 70 °C under vigorous stirring until a transparent solution was obtained. The resulting solution was then degassed by continuously flowing N₂ gas. Next, 115 mL methyl methacrylate was poured into the above solution while the temperature stayed at 70 °C. The mixtures were subsequently stirred at 70 °C for 1 h until a white suspension was obtained. After cooling to room T, the suspension was transferred to appropriate bottles for centrifugation (75 min), and the resulting solid obtained was washed with abundant deionized water. Then the precipitate was dried by a water bath at 80 °C for 5 h and then at room temperature for 48 h before ground well in fine powder (sample code PMMA).

2.2. Catalysts preparation

The three-dimensionally ordered macroporous (3DOM) LaCoO₃ and La_{0.8}Sr_{0.2}CoO_{3-δ} samples were prepared by a template method. A certain amount of La(NO₃)₃·6H₂O, Co(NO₃)₂·6H₂O, Sr(NO₃)₂ (only used for La_{0.8}Sr_{0.2}CoO_{3-δ} sample) metal precursors and deionized water were mixed under stirring for 1 h. Then ~2 g PMMA template was impregnated with the above solution (thoroughly wetted). Next, the excessive liquid was filtered and the solid was dried at room temperature for 24 h. The resulting solid was then calcined as follows: the first calcination step involved a heating rate of 1 °C/min up to 300 °C in N₂ gas flow, and the temperature of the solid was kept at 300 °C for 3 h. After cooling to room temperature, the calcination atmosphere was switched to air for the second calcination step that involved a heating rate of 1 °C/min up to 300 °C, and a stay at this temperature for 2 h. Subsequently, the solid was heated up in air to 900 °C and held for 4 h. The heating rate was kept at 1 °C/min. The obtained two perovskite materials, undoped and Sr-doped LaCoO₃ were denoted as LCO and LSCO, respectively.

LSCO-a sample was prepared by a selective removal of Sr method, in which the LSCO powder was immersed in diluted acetic acid (HAC) solution and kept for 10 h. The solid was then filtered, washed and dried at 60 °C overnight. The final product was denoted as LSCO-a.

2.3. Catalysts characterization

All the samples were characterized by means of powder X-ray diffraction (XRD), X-ray photoelectron spectroscopy (XPS), and

hydrogen temperature-programmed reduction (H₂-TPR) techniques, and N₂ physical adsorption measurements (77 K) for textural analysis. Details of the characterization procedures are provided in the Electronic Supporting Information (ESI).

2.4. Catalytic performance evaluation

The catalytic activities (in terms of toluene conversion) of toluene oxidation were evaluated in a continuous flow fixed-bed quartz micro-reactor (i.d. = 6.0 mm). The gaseous toluene was generated by passing N₂ gas flow through a bottle containing pure toluene chilled in an ice-water isothermal bath. The feed gas contained 2000 ppm toluene, 20% O₂, 3 or 5% H₂O (when needed) and N₂ (balance gas) at a total flow rate of 100 mL/min. The catalyst sample used was 0.05 g (40–60 mesh), giving a GHSV of ~120,000 mL/(g h). The concentration of toluene at the outlet of microreactor was monitored online by a gas chromatograph (Agilent 7890A) equipped with a flame ionization detector (FID) and a thermal conductivity detector (TCD). Further details are described in the ESI. When we evaluated the effect of GHSV on the catalytic activity for the LSCO-a sample, the amount of catalyst used was 0.025 g (GHSV = 240,000 mL/(g h) or 0.1 g (GHSV = 60,000 mL/(g h)). To test the catalytic stability of the LSCO-a sample, an uninterrupted reaction experiment was performed which involved three cycles (heating up and cooling down) of catalytic tests at the temperature range of 210–280 °C. The apparent activation energy of the toluene oxidation reaction (E_a, kJ/mol) was evaluated after conducting kinetic experiments in the temperature range of 210–250 °C, where toluene conversions were kept below 20%. Internal and external mass transport effects were checked according to the experimental criteria reported [28].

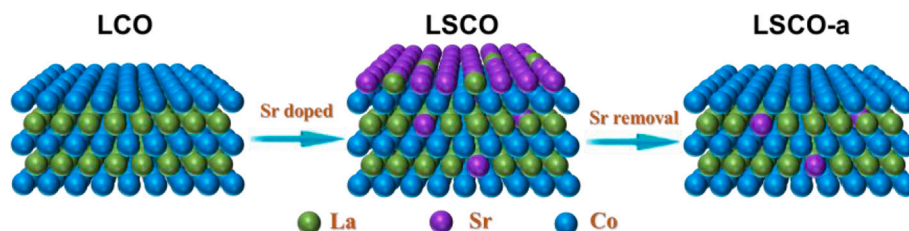
3. Results and discussion

3.1. Catalysts crystal structure

Powder X-ray diffraction (XRD) was used to investigate the crystal structure of the three perovskite-type materials as shown in Fig. S1 (ESI). It is found that the XRD peaks of these samples in the 10–80° 2θ range could be well correspond to the standard ABO₃ perovskites (refer to PDF #48-0123 and #46-0704). All these three samples were single-phase and of rhombohedral structure. Generally, the crystal structure (orthorhombic, rhombohedral or monoclinic) of perovskite is strongly dependent on the synthesis method. By adopting various preparation approaches with or without a template, rhombohedral and hexagonal perovskites could be generated. The structure of LSCO was the same as that of LCO, implying that Sr-doping did not change the crystal structure of the perovskite material. After HAC treatment, the intensity of XRD peaks for the LSCO-a catalyst sample was slightly weaker than that of LSCO, suggesting that the degree of crystallinity of the former perovskite decreased after HAC treatment.

3.2. Morphology and texture of perovskites

Fig. S2 illustrates the morphological differences of these three perovskite-type materials. It can be observed (Fig. S2(a)) that the PMMA



Scheme 1. Synthesis route of the LSCO-a catalyst sample.

spheres show a regular arrangement, whereas the LCO and LSCO solids possess high-quality chain-like ordered macroporous morphologies (Fig. S2(b) and S2(c), respectively). The average pore size was ~ 50 nm, and the average wall thickness ~ 22 nm. Fig. S2(d) reveal the change of the 3DOM structure after HAC treatment. The original smooth surface of the macropores became rumpled and the well-ordered structure became a little bit disordered. The surface area results (Table 1) from the N_2 adsorption–desorption isotherms and the pore-size distribution of the three samples (Fig. S3, ESI) were consistent with the information SEM images provided. The surface area was increased after Sr doping, ca. from 8.3 m^2/g (LCO) to 12.8 m^2/g (LSCO), while a further increase to 17.4 m^2/g (LSCO-a) after HAC treatment was noted. It is suggested that the shrinkage in volume of the treated materials could be responsible for the morphological and surface area changes. Normally, a porous structure of high surface area is beneficial for the improvement of its catalytic performance per gram basis due to the increased density of surface catalytic sites and for faster diffusion rates (increased pore size). Thus, the LSCO-a sample with the largest specific surface area (BET) and mean pore size facilitated toluene intra-particle diffusion rates and increased activity for toluene oxidation.

3.3. Catalyst surface composition and metal oxidation states

XPS experiments were carried out to provide information about surface elemental composition, including types of surface oxygen and cobalt species for the examined catalytic samples. Fig. 1 presents the Co $2p_{3/2}$ and O $1s$ XPS spectra recorded over the samples, and related estimated values of surface composition parameters are listed in Table 1. It is found that the surface Sr/La atom ratio for LSCO is 0.73, which is higher than the theoretical value 0.25. This indicates the enrichment of the surface of LSCO with Sr element. After HAC treatment, the surface Sr/La atom ratio for LSCO-a (0.26) shows an obvious reduction, which demonstrates the removal of Sr from the surface.

The XPS calculated value of La/Co ratio is also listed in Table 1. It is shown that La/Co atom ratio for LCO is 1.89, which is higher than the theoretical value (1.00). This result suggests that the native surface of LCO perovskite is preferentially occupied by La cations, which is in accord with earlier reports [25–27]. When LCO was doped with Sr the surface La/Co atom ratio for LSCO decreased to 1.37. This reduction could be attributed to the partially substituted La for Sr. The proportion for Sr substitution was 0.2, and the corresponding La/Co ratio should be 1.512. However, the surface La/Co atom ratio for LSCO is 1.37, which is lower than the theoretical value (1.512). This result indicates that bulk Sr element migrated on the sample surface, leading to the reduction of surface La composition. After HAC treatment, the surface La/Co atom ratio for LSCO-a becomes 1.13, which is the minimum value among the three samples. It is suggested that partial amount of surface La might had been removed by acid treatment after Sr substitution.

As shown in Fig. 1, surface Co^{3+} and Co^{2+} species, as well as surface lattice oxygen (O_{latt}), adsorbed oxygen (O_{ads} , e.g., O^{2-} , O_2^- , or O^-), and surface carbonates (CO_3^{2-}) are present on the surfaces of these three catalytic samples. The surface Co^{2+}/Co^{3+} and O_{ads}/O_{latt} atom ratios can markedly influence the VOCs catalytic oxidation performance of cobalt oxide. According to the quantitative analysis of the XPS spectra

provided, the surface Co^{2+}/Co^{3+} atom ratio was practically the same for the three solid surfaces but not in the case of O_{ads}/O_{latt} atom ratio. The latter varies in the 0.79–1.19 range (Table 1). One possible explanation for this behavior could be the charge imbalance created by the divalent Sr substitution for the trivalent La. Because the highest stable oxidation state for cobalt is +3, this charge imbalance can only be neutralized with O vacancies, which could be associated with the weakly bonded O_{ads} . After doping Sr into the LCO, the O_{ads} in the bulk LSCO should had been increased with the increase of O vacancies formation. But the surface of LSCO was covered by a large amount of SrO, which restricted the formation of surface O_{ads} . Therefore, the O_{ads}/O_{latt} ratio was decreased after LCO doping with Sr. After HAC treatment, surface Sr was removed to a large extent and the resulting LSCO-a solid caused an increased value for the O_{ads}/O_{latt} surface ratio. The increased specific surface area might have also played a role in the increase of O_{ads}/O_{latt} ratio after HAC treatment. The rise in surface active oxygen species concentration, especially for O_{ads} , might be linked to the enhanced catalytic performance of LSCO-a sample for the total oxidation of toluene.

H_2 -TPR experiments were conducted to investigate the reducibility of the samples, and their profiles are illustrated in Fig. 2. The hydrogen consumption over cobalt perovskites generally involves two temperature regions, i.e., at 300–500 °C corresponding to the reduction of Co^{3+} to Co^{2+} , and at 500–700 °C for the reduction of Co^{2+} to metallic cobalt (Co^0). The Co^{3+} reduction peak played an important role in the low-temperature reducibility of the catalysts. Compared with the LCO sample, the Co^{2+} reduction peak for the LSCO sample shifted from 600 to 570 °C as opposed to the Co^{3+} reduction peak for the LCO sample (ca. 403 and 441 °C) which appeared earlier than that of LSCO (ca. 422 °C). The latter result suggests that Sr doping did not improve the low temperature reducibility of LCO sample. For the LSCO-a sample, the Co^{3+} reduction peak shifted to a clearly lower temperature, ca. 338 °C. The improved low-temperature reducibility of the LSCO-a sample could be linked to the improvement of catalytic performance for toluene oxidation [29,30].

3.4. Catalytic performance

The evaluation of the catalytic activity of the three perovskite materials (LCO, LSCO and LSCO-a) in terms of toluene conversion for the oxidation of toluene in the 210–280 °C range is shown in Fig. 3(a). A blank activity test in the absence of catalyst showed that below 300 °C the conversion of toluene under the examined feed gas composition and GHSV was practically zero. The toluene conversion is increased with increasing reaction temperature for all three catalysts. The LSCO catalyst shows lower conversion values than the LCO sample in the whole temperature range. However, after the applied HAC treatment, the LSCO-a shows the best performance among the three samples, especially in the 220–260 °C range. In particular, at 250 °C the conversion of toluene is 80% for the LSCO-a compared to only 20% for the LSCO catalyst. Toluene was completely oxidized to CO_2 and H_2O over the three cobalt-based perovskite materials, and no partial oxidation products were detected in agreement to the very good carbon material balance (ca. 99.5%). T_{50} and T_{90} (the reaction temperature corresponding to toluene conversion of 50% and 90%, respectively) were used to

Table 1
Element composition, BET surface area, toluene oxidation activity, and apparent.

	XPS				S_{BET} (m^2/g)	toluene oxidation activity and apparent activation energy		
	Sr/La	La/Co	Co^{2+}/Co^{3+}	O_{ads}/O_{latt}		T_{50}	T_{90}	E_a
	molar ratio	molar ratio	molar ratio	molar ratio		(°C)	(°C)	(kJ/mol)
LCO	–	1.89	0.29	0.90	8.3	256	272	189
LSCO	0.73	1.37	0.32	0.79	12.8	264	295	203
LSCO-a	0.26	1.13	0.31	1.19	17.4	239	257	151

Activation energy (E_a) for the LCO, LSCO and LSCO-a catalytic materials.

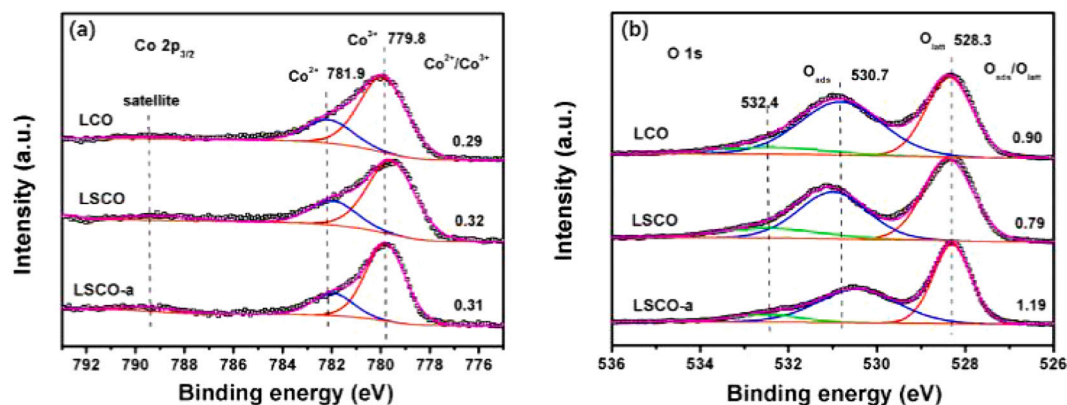


Fig. 1. (a) Co $2p_{3/2}$ and (b) O $1s$ XPS spectra of the LCO, LSCO and LSCO-a samples.

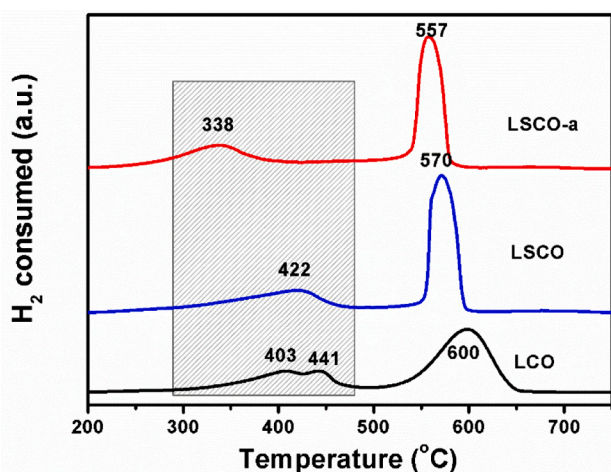


Fig. 2. H_2 -TPR profiles of the LCO, LSCO and LSCO-a samples.

compare the catalytic activities of the three samples. For the LCO, LSCO and LSCO-a samples, the values of T_{50} obtained were 256, 264, and 239 °C, respectively, and of T_{90} were 272, 295 and 257 °C, respectively (Table 1). Therefore, it can be deduced that the activities of the three samples enhanced in the order of LSCO < LCO < LSCO-a. The oxidation of toluene at low temperatures usually occurs on the surface transition metal cation sites (such as Co cations). The surface of LSCO sample was preferentially occupied by Sr cations, as proved by the XPS results, and active Co sites were partially covered causing reduction in activity. After the HAC treatment, surface Sr was removed to a large extent, and

exposed surface Co cations concentration increased significantly, giving rise to the improved performance illustrated in Fig. 3(a). By comparing the catalytic activity and characterization results presented in this work, it can be found that there was an obvious correlation of surface oxygen species concentration, and low-temperature reducibility with toluene oxidation activity. After normalizing the activity results shown in Fig. 3 (a) per unit surface area, the same activity trend among the three catalytic materials remained. The apparent activation energy (E_a) was estimated, and results are presented in Fig. 3(b) using the Arrhenius relationship (R^2 values better than 0.991). The LSCO-a catalyst with the lowest E_a value exhibits the highest catalytic activity for toluene combustion at low temperatures. The differences in E_a values are most likely generated by the intrinsic activity of surface oxygen species. It should be noted that the LSCO-a sample possessed the highest O_{ads}/O_{latt} ratio.

It is well known that the presence of H_2O in flue gas affects toluene oxidation activity on the perovskites catalysts. The effects of H_2O (3% and 5%) on the activity of the LSCO-a at 240 and 260 °C were studied and results are shown in Fig. S4. It can be observed that there was a slight decrease in toluene conversion upon introduction of water in the feed gas stream over the LSCO-a catalyst, which was stabilized after ~ 2 h in the the stream with water. At 240 °C, the final decrease of toluene conversion after adding 3% and 5% H_2O was 2.4% and 3.2%, respectively. At 260 °C, the corresponding values were 4.6% and 7.2%, respectively. It should also be noted that toluene conversion was almost restored after excluding H_2O from the reactant feed gas stream. These results suggest that the LSCO-a sample possessed good tolerance to H_2O , which is promising for practical applications.

To test the catalytic stability of the LSCO-a sample, an uninterrupted reaction experiment was performed which involved three consecutive runs of catalytic tests (heating up and cooling down), and results are

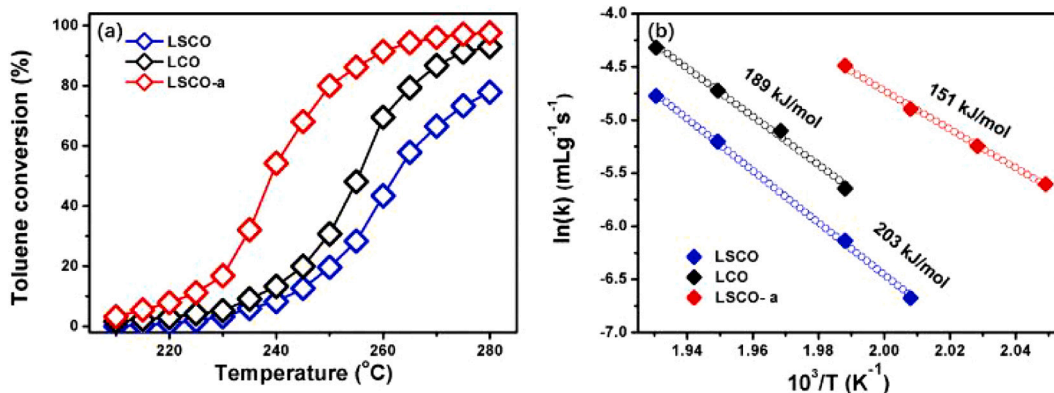


Fig. 3. (a) Activity profiles and (b) Arrhenius plots of the LCO, LSCO and LSCO-a samples. Reaction conditions: 2000 ppm toluene, 20% O_2 , and N_2 (balance gas), GHSV = 120,000 mL/(g h).

shown in Fig. S5 (ESI). The running time of the whole stability test was ~45 h, and the observed result is that the activity of LSCO-a remained practically unchanged within 45 h of reaction. The influence of GHSV on the toluene conversion was also investigated and results are presented in Fig. S6 (ESI). In the case of LSCO-a sample, the T_{50} and T_{90} values were 239 and 257 °C at GHSV = 120,000 mL/(g h), respectively. These T_{50} and T_{90} values are 12 and 16 °C lower, respectively, than those achieved at the highest GHSV of 240,000 mL/(g h). When the GHSV was decreased from 120,000 to 60,000 mL/(g h), the toluene conversions increased. This behavior is characteristic of a relatively fast kinetic rate of toluene oxidation compared to the rates of mass transport.

4. Conclusions

LSCO-a sample was prepared by treating LSCO with diluted acetic acid. This method eliminated the adverse effect on the catalytic activity brought by the formation of SrO segregation on the surface of LSCO catalyst. The LSCO-a sample showed significantly enhanced catalytic activity in toluene oxidation than LCO and LSCO samples, which was linked to the higher surface concentration of oxygen species and better low-temperature oxygen reducibility. In addition, the LSCO-a sample exhibited a good stability during 45 h time-on-stream, and also good tolerance to water vapor. The present results could provide a thought to design high-performance perovskite catalysts in VOCs oxidation.

Declaration of competing interest

The authors declare that they have no known competing financial interests or personal relationships that could have appeared to influence the work reported in this paper.

Appendix A. Supplementary data

Supplementary data to this article can be found online at <https://doi.org/10.1016/j.catcom.2021.106314>.

References

- [1] J.-H. Park, A.H. Goldstein, J. Timkovsky, S. Fares, R. Weber, J. Karlik, R. Holzinger, *Science* 341 (2013) 643–647.
- [2] J. Yoon, S.K. Chae, J.-M. Kim, *J. Am. Chem. Soc.* 129 (2007) 3038–3039.
- [3] T. Barakat, J.C. Rooke, E. Genty, R. Cousin, S. Siffert, B.-L. Su, *Energy Environ. Sci.* 6 (2013) 371–391.
- [4] S.C. Kim, W.G. Shim, *J. Hazard. Mater.* 154 (2008) 310–316.
- [5] K.M. Parida, N. Sahu, A.K. Tripathi, V.S. Kamble, *Environ. Sci. Technol.* 44 (2010) 4155–4160.
- [6] H. Rotter, M.V. Landau, M. Herskowitz, *Environ. Sci. Technol.* 39 (2005) 6845–6850.
- [7] T.-K. Tseng, H. Chu, H.-H. Hsu, *Environ. Sci. Technol.* 37 (2003) 171–176.
- [8] R. Wang, J. Li, *Environ. Sci. Technol.* 44 (2010) 4282–4287.
- [9] T. Masui, H. Imadzu, N. Matsuyama, N. Imanaka, *J. Hazard. Mater.* 176 (2010) 1106–1109.
- [10] V.P. Santos, S.A.C. Carabineiro, P.B. Tavares, M.F.R. Pereira, J.J.M. Órfão, J. L. Figueiredo, *Appl. Catal. B* 99 (2010) 198–205.
- [11] W.G. Shim, J.W. Lee, S.C. Kim, *Appl. Catal. B* 84 (2008) 133–141.
- [12] Y. Nishihata, J. Mizuki, T. Akao, H. Tanaka, M. Uenishi, M. Kimura, T. Okamoto, N. Hamada, *Nature* 418 (2002) 164–167.
- [13] J.J. Zhu, A. Thomas, *Appl. Catal. B* 92 (2009) 225–233.
- [14] C.H. Kim, G. Qi, K. Dahlberg, W. Li, *Science* 327 (2010) 1624–1627.
- [15] J. Zhu, H. Li, L. Zhong, P. Xiao, X. Xu, X. Yang, Z. Zhao, J. Li, *ACS Catal.* 4 (2014) 2917–2940.
- [16] C. Zhang, Y. Guo, Y. Guo, G. Lu, A. Boreave, L. Retailleau, A. Baylet, A. Giroir-Fendler, *Appl. Catal. B* 148–149 (2014) 490–498.
- [17] C. Zhang, W. Hua, C. Wang, Y. Guo, Y. Guo, G. Lu, A. Baylet, A. Giroir-Fendler, *Appl. Catal. B* 134–135 (2013) 310–315.
- [18] J. Xu, J. Liu, Z. Zhao, J. Zheng, G. Zhang, A. Duan, G. Jiang, *Catal. Today* 153 (2010) 136–142.
- [19] Y.G. Wang, J.W. Ren, Y.Q. Wang, F.Y. Zhang, X.H. Liu, Y. Guo, G.Z. Lu, *J. Phys. Chem. C* 112 (2008) 15293–15298.
- [20] Y.J. Zhu, D. Wang, F.L. Yuan, G. Zhang, H.G. Fu, *Appl. Catal. B* 82 (2008) 255–263.
- [21] J. Zhang, D. Tan, Q. Meng, X. Weng, Z. Wu, *Appl. Catal. B* 172–173 (2015) 18–26.
- [22] D.L. Chen, K.L. Pan, M.B. Chang, *J. Environ. Sci.* 56 (2017) 131–139.
- [23] Z. Feng, Y. Yacoby, W.T. Hong, H. Zhou, M.D. Biegalski, H.M. Christen, Y. Shao-Horn, *Energy Environ. Sci.* 7 (2014) 1166–1174.
- [24] M. Kubicek, G.M. Rupp, S. Huber, A. Penn, A.K. Opitz, J. Bernardi, M. Stöger-Pollach, H. Hutter, J. Fleig, *Phys. Chem. Chem. Phys.* 16 (2014) 2715–2726.
- [25] Y. Wei, L. Ni, M. Li, J. Zhao, *Catal. Today* 297 (2017) 188–192.
- [26] W. Si, Y. Wang, S. Zhao, F. Hu, J. Li, *Environ. Sci. Technol.* 50 (2016) 4572–4578.
- [27] W. Si, Y. Wang, Y. Peng, J. Li, *Angew. Chem. Int. Ed.* 54 (2015) 7954–7957.
- [28] C. Perego, S. Peratello, *Catal. Today* 52 (1999) 133–145.
- [29] S. Stefa, M. Lykaki, V. Binas, P.K. Pandis, V.N. Stathopoulos, M. Konsolakis, *Appl. Sci.* 10 (2020) 7605, <https://doi.org/10.3390/app10217605>.
- [30] S. Stefa, M. Lykaki, D. Fragkouli, V. Binas, P.K. Pandis, V.N. Stathopoulos, M. Konsolakis, *Processes* 8 (2020) 847, <https://doi.org/10.3390/pr8070847>.